



OPEN Fast algorithm and new potential formula represented by Chebyshev polynomials for an $m \times n$ globe network

Yufan Zhou¹, Yanpeng Zheng^{2✉}, Xiaoyu Jiang¹ & Zhaolin Jiang^{3✉}

Resistor network is widely used. Many potential formulae of resistor networks have been solved accurately, but the scale of data is limited by manual calculation, and numerical simulation has become the trend of large-scale operation. This paper improves the general solution of potential formula for an $m \times n$ globe network. Chebyshev polynomials are introduced to represent new potential formula of a globe network. Compared with the original potential formula, it saves time to calculate the potential. In addition, an algorithm for computing potential by the famous second type of discrete cosine transform (DCT-II) is also proposed. It is the first time to be used for machine calculation. Moreover, it greatly increases the efficiency of computing potential. In the application of this new potential formula, the equivalent resistance formulae in special cases are given and displayed by three-dimensional dynamic view. The new potential formulae and the proposed fast algorithm realize large-scale operation for resistor networks.

With the development of natural science, people have encountered various new problems. According to the complexity of the problem, solutions emerge in endlessly. Researches show that a host of problems can be solved by establishing resistor network model^{1–10} and neural network model^{11–17}. In the past few years, many results have been achieved in the study of resistor networks. For example, the establishment of graph theory, the researches on Laplacian matrix (*LM*) method of resistor network, infinite network, finite network, and corner-to-corner resistance and so on^{7–10,18–31}. Shi^{11,12} et al. studied a novel discrete-time recurrent neural network. Liu¹³ et al. and Sun¹⁴ et al. proposed different types of the zeroing neural network. And Jin^{15–17} et al. studied an innovative control theory stimulated gradient neural network algorithm.

In recent years, Tan^{32–43} proposed the Recursion-Transform (*RT*) method which is different from the Laplacian matrix method. It only depends on one matrix and one direction, and the calculation is simpler. In 2013, Tan³² studied the problem of two-point resistance on cobweb with a $2r$ boundary, which has never been solved before. Under finite and infinite conditions, the $m \times n$ cobweb general formula of resistance between any two nodes is proposed. In 2014, Tan^{36,38} made a new breakthrough and introduced the equivalent resistance of the globe network and fan network model by *RT* method. Shortly after that many researches on resistor networks are based on *RT* method. *RT* method needs eigenvalues of a tridiagonal matrix to represent the potential formula. At present, there have been many results on tridiagonal matrices^{45–51}, which are also widely used. It can be said that it is a powerful tool to solve the resistor network^{33–43}.

In 2018, Tan⁴⁴ proposed an $m \times n$ globe network, as shown in Fig. 1. The resistances in the latitude and longitude directions are r and r_0 , respectively, where m and n are the resistance numbers along the latitude and longitude directions. The nodes of the network are represented by coordinates $\{x, y\}$. Considering $O_0 = 0$ as the origin of the coordinate system, the potential of node $d(x, y)$ is $U_{m \times n}(x, y)$ as shown in Fig. 2. The potential of any node in the $m \times n$ globe network is as follows

$$\frac{U_{m \times n}(x, y)}{J} = \frac{y(y_1 - y_2)}{mn} r_0 + \frac{2r}{m} \sum_{i=2}^m \frac{\beta_{x_1, x}^{(i)} S_{y_1, i} - \beta_{x_2, x}^{(i)} S_{y_2, i}}{\lambda_i^n + \bar{\lambda}_i^n - 2} S_{y, i}, \quad (1)$$

where

¹School of Information Science and Engineering, Linyi University, Linyi 276000, China. ²School of Automation and Electrical Engineering, Linyi University, Linyi 276000, China. ³School of Mathematics and Statistics, Linyi University, Linyi 276000, China. ✉email: zhengyanpeng0702@sina.com; jzh1208@sina.com

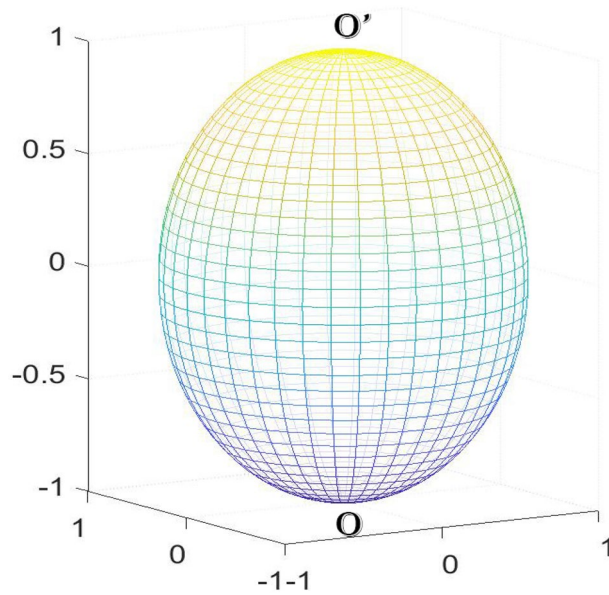


Figure 1. An $m \times n$ globe network which has n longitude and $m - 1$ latitude. The resistances in the longitude and latitude directions are r_0 and r , respectively.

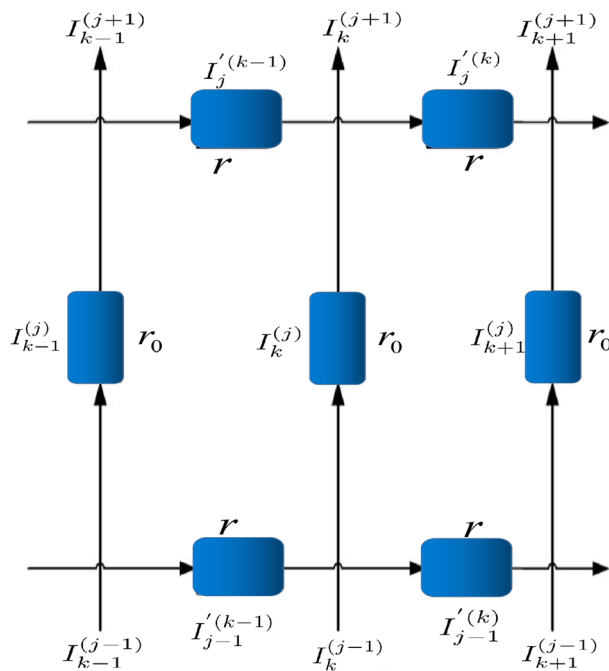


Figure 2. Segment of the globe network with current directions and parameters.

$$S_{k,i} = \sin(y_k \theta_i), \theta_i = (i - 1)\pi/m, \tag{2}$$

$$\beta_{x_s, x_k}^{(i)} = F_{n-|x_s-x_k|} + F_{|x_s-x_k|}, F_k^{(i)} = (\lambda_i^k - \bar{\lambda}_i^k)/(\lambda_i - \bar{\lambda}_i), \tag{3}$$

$$\lambda_i = 1 + b - b \cos \theta_i + \sqrt{(1 + b - b \cos \theta_i)^2 - 1}, \tag{4}$$

$$\bar{\lambda}_i = 1 + b - b \cos \theta_i - \sqrt{(1 + b - b \cos \theta_i)^2 - 1}, \quad b = r/r_0.$$

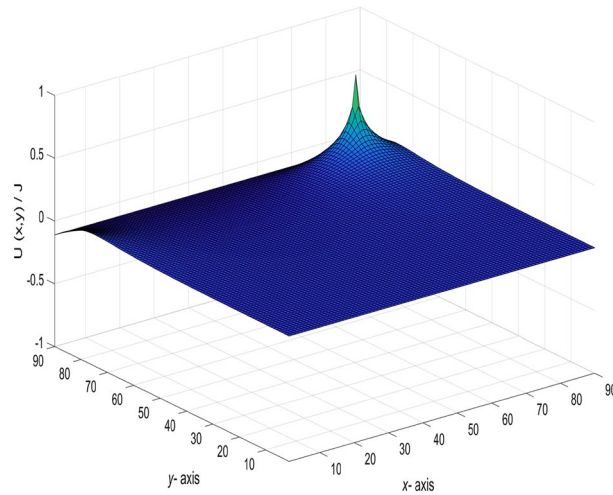


Figure 3. A 3D dynamic view for the changing graph of $U_{90 \times 90}(x, y)/J$ with the current input and output point change.

New formula of potential represented by Chebyshev polynomials

Since the potential formula (1) contains exponential function operation, it is less efficient to calculate potential of globe resistor networks by computer. The purpose of this section is to give an improved potential formula of the globe network⁴⁴, i.e. a new formula of potential expressed by Chebyshev polynomial of the second class is given⁵³. it saves time to calculate the potential by computer.

Let the current J from $d_1(x_1, y_1)$ to $d_2(x_2, y_2)$, the potential formula of two nodes in an $m \times n$ resistor network can be written as

$$\frac{U_{m \times n}(x, y)}{J} = \frac{y(y_1 - y_2)}{mn} r_0 + \frac{2r}{m} \sum_{j=2}^m \frac{\gamma_{x_1, x}^{(j)} C_{y_1, j} - \gamma_{x_2, x}^{(j)} C_{y_2, j}}{t_j U_{n-1}^{(j)} - 2U_{n-2}^{(j)} - 2} C_{y, j}, \tag{5}$$

where

$$\gamma_{x_s, x_k}^{(j)} = U_{n-|x_s-x_k|-1}^{(j)} + U_{|x_s-x_k|-1}^{(j)}, \quad s = 1, 2, \tag{6}$$

$$C_{p, j} = \sin\left(\frac{p(j-1)\pi}{m}\right), \quad p = y_1, y_2, y, \tag{7}$$

$$t_j = 2 + \frac{2r}{r_0} - \frac{2r}{r_0} \cos\left(\frac{(j-1)\pi}{m}\right), \tag{8}$$

$$U_k^{(j)} = U_k^{(j)}(\cos \psi_j) = \frac{\sin(k+1)\psi_j}{\sin(\psi_j)}, \quad \psi_j = \arccos\left(1 + \frac{r}{r_0} - \frac{r}{r_0} \cos\left(\frac{(j-1)\pi}{m}\right)\right), \tag{9}$$

$$k = n - |x_1 - x|, |x_1 - x|, n - |x_2 - x|, |x_2 - x|, n - 1, n - 2, \quad j = 1, 2, \dots, m.$$

In particular, the input and output points can be one or more, so formula (5) applies to all coordinate points (x_k, y_k) ($0 \leq k \leq n$). Therefore, p can also be y_3, y_4, \dots, y_k .

Suppose that $O_0 = 0$, then calculating the node potential between any two points by Ohm's law can be described as

$$U_{m \times n}(x, y) = U(0, 0) - r_0 \sum_{j=1}^y I_x^{(j)} = -r_0 \sum_{j=1}^y I_x^{(j)}, \tag{10}$$

where $I_x^{(j)}$ is denoted by the current in the vertical direction.

Base on formula (5), using the visualization of data to realize the dynamic visualization of the potential change. With the change of the current input and output point change, the potential change of any two nodes is shown in Fig. 3.

Three terms recurrence sequence and discrete cosine transform

In this section, in order to improve the actual performance and realize the fast algorithm, the three terms recurrence sequence represented by Chebyshev polynomial of the second class and two types of discrete cosine transform are introduced.

The three terms recurrence sequence is defined by the following conditions:

$$W_k = dW_{k-1} - qW_{k-2}, \quad W_0 = A, \quad W_1 = B, \tag{11}$$

where $k \in \mathbf{N}$, $k \geq 2$, $A, B, d, q \in \mathbf{C}$, \mathbf{N} is the set of all natural numbers and \mathbf{C} is the set of all complex numbers. The three terms recurrence sequence⁵² represented by Chebyshev polynomial of the second class is

$$W_k = (\sqrt{q})^k \left(\frac{B}{\sqrt{q}} U_{k-1} \left(\frac{d}{2\sqrt{q}} \right) - A U_{k-2} \left(\frac{d}{2\sqrt{q}} \right) \right), \tag{12}$$

where

$$U_k = \frac{\sin(k+1)\psi}{\sin \psi}, \quad \psi = \arccos\left(\frac{d}{2\sqrt{q}}\right) \in \mathbf{C}, \tag{13}$$

is the Chebyshev polynomial of the second class⁵³.

Remark Based on the above formula, how to replace Eqs. (1), (2), (3) and (4) with Eqs. (5), (6), (7) and (9) will be showed, respectively. According to the equation (4), $\lambda_j + \bar{\lambda}_j = t_j$ and $\lambda_j \cdot \bar{\lambda}_j = 1$ are obtained. Take it into the equation (11), and a three term recursive formula is obtained

$$F_k^{(j)} = t_j F_{k-1}^{(j)} - F_{k-2}^{(j)}, \quad F_0^{(j)} = 0, \quad F_1^{(j)} = 1, \tag{14}$$

where $d = t_j$, $q = 1$, t_j and $F_k^{(j)}$ are the same as Eqs. (8) and (3), respectively. By Eq. (14) and formula (12), the replacement result can be obtained

$$F_k^{(j)} = (\lambda_j^k - \bar{\lambda}_j^k) / (\lambda_j - \bar{\lambda}_j) = U_{k-1}^{(j)} \left(\frac{t_j}{2} \right). \tag{15}$$

Similarly, Let

$$Q_n^{(j)} = \lambda_j^n + \bar{\lambda}_j^n, \tag{16}$$

where $Q_0^{(j)} = 2$, $Q_1^{(j)} = t_j$. Then the recursive relation of $Q_n^{(j)}$ is obtained as follows

$$Q_n^{(j)} = t_j Q_{n-1}^{(j)} - Q_{n-2}^{(j)}, \quad Q_0^{(j)} = 2, \quad Q_1^{(j)} = t_j, \tag{17}$$

where $d = t_j$, $q = 1$, t_j and $Q_n^{(j)}$ are the same as Eqs. (8) and (16), respectively. By Eq. (17) and formula (12), the replacement result can be obtained as follows

$$Q_n^{(j)} = \lambda_j^n + \bar{\lambda}_j^n = t_j U_{n-1} \left(\frac{t_j}{2} \right) - U_{n-2} \left(\frac{t_j}{2} \right). \tag{18}$$

According to Eqs. (1), (3),(15) and (18), a new potential formula (5) is got.

In order to obtain a fast numerical algorithm for computing the potential, the orthogonal diagonalization of the matrix \mathbf{B}_m is given.

$$\mathbf{B}_m = \begin{pmatrix} 2+b & -b & 0 & \dots & 0 \\ -b & 2(1+b) & -b & \ddots & \vdots \\ 0 & \ddots & \ddots & \ddots & 0 \\ \vdots & \ddots & -b & 2(1+b) & -b \\ 0 & \dots & 0 & -b & 2+b \end{pmatrix}_{m \times m}, \tag{19}$$

where $b = r/r_0$.

Then the eigenvalues t_1, \dots, t_m of \mathbf{B}_m are given by

$$t_j = 2 + 2b - 2b \cos \frac{(j-1)\pi}{m}, \quad j = 1, 2, \dots, m, \tag{20}$$

and the corresponding eigenvectors $\zeta^{(j)} = (\zeta_1^{(j)}, \dots, \zeta_m^{(j)})^\dagger$ are given by

$$\zeta_k^{(j)} = \sqrt{\frac{2}{m}} d_j \cos \frac{(2k-1)(j-1)\pi}{2m}, \quad k = 1, 2, \dots, m, j = 1, 2, \dots, m, \tag{21}$$

where $d_j = \begin{cases} 1, & j \neq 1, \\ \frac{\sqrt{2}}{2}, & j = 1. \end{cases}$

Let

$$\mathbb{C}_m^{III} = \left(\sqrt{\frac{2}{m}} d_j \cos \frac{(2k-1)(j-1)\pi}{2m} \right)_{k,j=1}^m, \tag{22}$$

where $d_j = \begin{cases} 1, & j \neq 1, \\ \frac{\sqrt{2}}{2}, & j = 1. \end{cases}$

Obviously, the matrix \mathbb{C}_m^{III} is the famous third type of discrete cosine transform (DCT-III)⁵⁴⁻⁵⁷. \mathbb{C}_m^{III} is an orthogonal matrix and the inverse of \mathbb{C}_m^{III} is actually \mathbb{C}_m^{II} , i.e.

$$(\mathbb{C}_m^{III})^{-1} = (\mathbb{C}_m^{III})^T = \mathbb{C}_m^{II}, \tag{23}$$

where the orthogonal matrix \mathbb{C}_m^{II} is the famous second type of discrete cosine transform (DCT-II)⁵⁴⁻⁵⁷.

By calculation we obtain the orthogonal diagonalization of the matrix \mathbf{B}_m as follows

$$(\mathbb{C}_m^{III})^{-1} \mathbf{B}_m (\mathbb{C}_m^{III}) = \text{diag}(t_1, t_2, \dots, t_m), \tag{24}$$

i.e.

$$\mathbf{B}_m = (\mathbb{C}_m^{III}) \text{diag}(t_1, t_2, \dots, t_m) (\mathbb{C}_m^{III})^{-1}, \tag{25}$$

where $t_j, j = 1, 2, \dots, m$ are given by Eq. (20).

Tan⁴⁴ used Kirchhoff's law to analyze the resistor network and to establish the resistor network model. The following general matrix equation is

$$\mathbf{I}_{k+1} = \mathbf{B}_m \mathbf{I}_k - \mathbf{I}_{k-1} - b \mathbf{H}_y \delta_{k,x}, \tag{26}$$

where \mathbf{B}_m is given by Eq. (19), the function $\delta_{k,x}$ is defined as: $\delta_{k,x}(x = k) = 1, \delta_{k,x}(x \neq k) = 0, \mathbf{I}_k$ and \mathbf{H}_x are the $m \times 1$ column matrices, and can be written as

$$\mathbf{I}_k = [I_k^{(1)}, I_k^{(2)}, \dots, I_k^{(m)}]^T \quad (0 \leq k \leq n), \tag{27}$$

$$(\mathbf{H}_1)_k = J(-\delta_{k,y_1} + \delta_{k,y_1+1}), \quad (\mathbf{H}_2)_k = J(\delta_{k,y_2} - \delta_{k,y_2+1}). \tag{28}$$

To solve the Eq. (26), using the matrix transformation method to multiply \mathbb{C}_m^{III} at the same time. Through Eq. (24) and the transformed matrix equation we appoint

$$\sqrt{\frac{m}{2}} \mathbb{C}_m^{III} \mathbf{I}_k = \mathbf{W}_k \text{ and } \mathbf{I}_k = \sqrt{\frac{2}{m}} (\mathbb{C}_m^{III})^T \mathbf{W}_k = \sqrt{\frac{2}{m}} \mathbb{C}_m^{II} \mathbf{W}_k, \tag{29}$$

where the $m \times 1$ column matrix \mathbf{W}_k is

$$\mathbf{W}_k = [W_k^{(1)}, W_k^{(2)}, \dots, W_k^{(m)}]^T \quad (0 \leq k \leq n). \tag{30}$$

Based on the Chebyshev polynomial of the second class, the general solution formula of current is rewritten. When $j = 1$, the following formula is obtained

$$W_k^{(1)} = \frac{J(y_2 - y_1)}{n\sqrt{2}}, \quad (0 \leq k \leq n). \tag{31}$$

When $j \geq 2$, the following formula is obtained

$$W_x^{(j)} = bJ \frac{\gamma_{x_1,x}^{(j)} \varsigma_{1j} + \gamma_{x_2,x}^{(j)} \varsigma_{2j}}{t_j U_{n-1}^{(j)} - 2U_{n-2}^{(j)} - 2}, \quad (0 \leq x \leq n), \tag{32}$$

where $\gamma_{x_s,x_k}^{(j)}$ is equal to Eq. (6), $\varsigma_{1j} = -2 \sin(\frac{(j-1)\pi}{2m}) \sin(\frac{y_1(j-1)\pi}{m})$, and $\varsigma_{2j} = 2 \sin(\frac{(j-1)\pi}{2m}) \sin(\frac{y_2(j-1)\pi}{m})$.

Displaying of some special and interesting potential formulae

Since formula (5) is a general potential conclusion of a globe network including all cases, some special conditions in formula (5) and a series of fascinating results under various parameters will be displayed. In the following, assuming that the potential reference at point $O(0, 0)$ is $U(0, 0) = 0$.

Special 1. Suppose the current J flows in from the origin $d_1(x_1, y_1)$ and out from $d_2(x_2, y_2) = O(0, 0)$, the potential of any two points can be written as

$$\frac{U_{m \times n}(x, y)}{J} = \frac{\gamma y_1}{mn} r_0 + \frac{2r}{m} \sum_{j=2}^m \left(\frac{\sin(\frac{y_1(j-1)\pi}{m}) \sin(\frac{y(j-1)\pi}{m})}{t_j U_{n-1}^{(j)} - 2U_{n-2}^{(j)} - 2} \right) \gamma_{x_1,x}^{(j)}, \tag{33}$$

where $\gamma_{x_s,x_k}^{(j)} = U_{n-|x_s-x_k|-1}^{(j)} + U_{|x_s-x_k|-1}^{(j)}$ is defined in Eq. (6), and $U_k^{(j)}$ is the same as Eq. (9).

When $m = n = 90, j = 10, x_1 = y_1 = 50, x_2 = y_2 = 0$, and $r_0 = r = 1$, the following formula is obtained

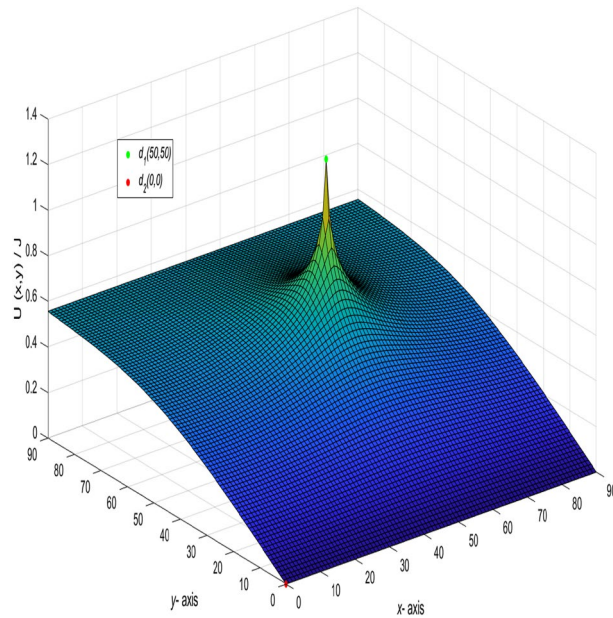


Figure 4. The process of forming a 3D dynamic view for $U_{90 \times 90}(x, y)/J$ in Eq. (34).

$$\frac{U_{90 \times 90}(x, y)}{J} = \frac{y}{162} + \frac{1}{45} \sum_{j=2}^{90} \left(\frac{\sin(\frac{5(j-1)\pi}{9}) \sin(\frac{(j-1)\pi}{90})}{t_j U_{89}^{(j)} - 2U_{88}^{(j)} - 2} \right) \gamma_{50,x}^{(j)} \tag{34}$$

where

$$t_j = 4 - 2 \cos \frac{(j-1)\pi}{90}, \tag{35}$$

$$\gamma_{50,x}^{(j)} = U_{89-|50-x|}^{(j)} + U_{|50-x|-1}^{(j)}, \tag{36}$$

$$U_k^{(j)} = U_k^{(j)} (\cos \psi_j) = \frac{\sin(k+1)\psi_j}{\sin(\psi_j)}, \quad \psi_j = \arccos(2 - \cos \frac{(j-1)\pi}{90}), \tag{37}$$

$$k = 89 - |50 - x|, |50 - x| - 1, 89, 88, \quad j = 1, 2, \dots, 90.$$

And a 3D dynamic view is shown in Fig. 4 by Matlab.

Special 2. Consider an arbitrary $m \times n$ globe network as shown in Fig. (1). Assume the electric current J outflow the network from the pole $d_2(x_2, y_2)$, and the current J input at the node $d_1(x_1, y_1) = O(0, 0)$, the potential of an arbitrary node $d(x, y)$ can be written as

$$\frac{U_{m \times n}(x, y)}{J} = -\frac{yy_2}{mn} r_0 + \frac{2r}{m} \sum_{j=2}^m \left(-\frac{\sin(\frac{y_2(j-1)\pi}{m}) \sin(\frac{y(j-1)\pi}{m})}{t_j U_{n-1}^{(j)} - 2U_{n-2}^{(j)} - 2} \right) \gamma_{x_2,x}^{(j)} \tag{38}$$

where $\gamma_{x_s, x_k}^{(j)}$ is defined in Eq. (6), and $U_k^{(j)}$ is the same as Eq. (9).

In the network with $m = 90$ and $n = 90$, the current flows in from $(x_1, y_1)(x_1 = 0, y_1 = 0)$ and out from $(x_2, y_2)(x_2 = 30, y_2 = 30)$. Let $r_0 = r = 1$ and $J = 10$, the formula is deduced.

$$\frac{U_{90 \times 90}(x, y)}{J} = -\frac{y}{270} + \frac{1}{45} \sum_{j=2}^{90} \left(\frac{-\sin(\frac{(j-1)\pi}{3}) \sin(\frac{(j-1)\pi}{90})}{t_j U_{89}^{(j)} - 2U_{88}^{(j)} - 2} \right) \gamma_{30,x}^{(j)} \tag{39}$$

where

$$\gamma_{30,x}^{(j)} = U_{89-|30-x|}^{(j)} + U_{|30-x|-1}^{(j)}, \tag{40}$$

t_j and $U_k^{(j)}$ are the same as Eqs. (35) and (37), respectively, $k = 89 - |30 - x|, |30 - x| - 1, 89, 88, \quad j = 1, 2, \dots, 90$. And a 3D dynamic view is shown in Fig. 5 by Matlab.

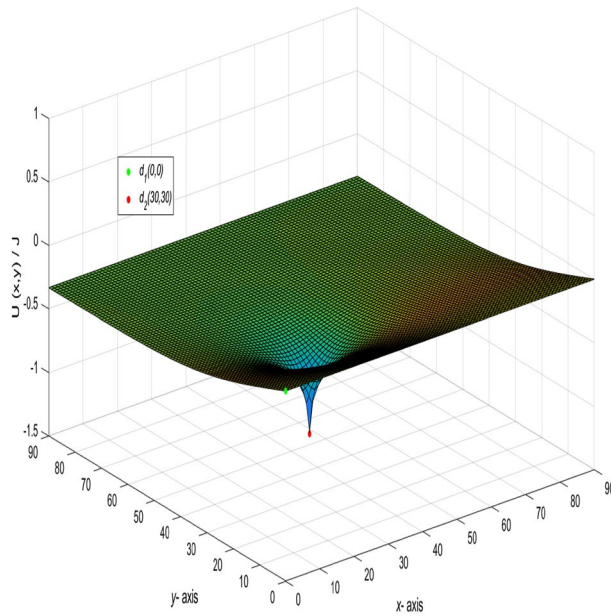


Figure 5. The process of forming a 3D dynamic view for $U_{90 \times 90}(x, y)/J$ in Eq. (39).

Special 3. Presume that when the current J is injected at node $d_1(x_1, y_1)$ and withdrawn at node $d_2(x_2, y_2)$ ($x_2 = y_1, y_2 = x_1$), the potential of any node $d(x, y)$ is

$$\frac{U_{m \times n}(x, y)}{J} = \frac{yy_1}{mn}r_0 + \frac{2r}{m} \sum_{j=2}^m \frac{(U_{n-x}^{(j)} + U_x^{(j)}) \sin(\frac{y_1(j-1)\pi}{m}) \sin(\frac{y(j-1)\pi}{m})}{t_j U_{n-1}^{(j)} - 2U_{n-2}^{(j)} - 2}, \tag{41}$$

where t_j is defined in Eq. (8), and $U_k^{(j)}$ is the same as Eq. (9).

In the scale of $m \times n(90 \times 90)$, we get $J = 10, x_1 = y_2 = 0, x_2 = y_1 = 30$, and $r_0 = r = 1$, the following formula is

$$\frac{U_{90 \times 90}(x, y)}{J} = \frac{y}{270} + \frac{1}{45} \sum_{j=2}^{90} \frac{(U_{90-x}^{(j)} + U_x^{(j)}) \sin(\frac{(j-1)\pi}{3}) \sin(\frac{y(j-1)\pi}{90})}{t_j U_{89}^{(j)} - 2U_{88}^{(j)} - 2}, \tag{42}$$

where t_j and $U_k^{(j)}$ are the same as Eq. (35) and Eq. (37), respectively, and $k = 90 - x, x, 89, 88, j = 1, 2, \dots, 90$. And a 3D dynamic view is shown in Fig. 6 by Matlab.

Special 4. When we inject current J at node $d_1(x_1, y_1)$ and exit the current J at node $d_2(x_1, y_2)$ ($x_2 = x_1$), the potential of an arbitrary node $d(x, y)$ is

$$\frac{U_{m \times n}(x, y)}{J} = \frac{y(y_1 - y_2)}{mn}r_0 + \frac{2r}{m} \sum_{j=2}^m \left(\frac{(C_{y_1,j} - C_{y_2,j})C_{y,j}}{t_j U_{n-1}^{(j)} - 2U_{n-2}^{(j)} - 2} \right) \gamma_{x_1,x}^{(j)}, \tag{43}$$

where $C_{k,j}, U_k^{(j)}$ and $\gamma_{x_1,x}^{(j)}$ are equal to Eqs. (7), (9) and Eq. (6), respectively.

When $m = n = 90, J = 10, x_1 = x_2 = y_1 = 50, y_2 = 30$, and $r_0 = r = 1$, the following formula is obtained

$$\frac{U_{90 \times 90}(x, y)}{J} = \frac{y}{405} + \frac{1}{45} \sum_{j=2}^{90} \left(\frac{(C_{50,j} - C_{30,j})C_{y,j}}{t_j U_{89}^{(j)} - 2U_{88}^{(j)} - 2} \right) \gamma_{50,x}^{(j)}, \tag{44}$$

where

$$\begin{aligned} C_{50,j} &= \sin\left(\frac{5(j-1)\pi}{9}\right), \\ C_{30,j} &= \sin\left(\frac{(j-1)\pi}{3}\right), \end{aligned} \tag{45}$$

$t_j, U_k^{(j)}$ and $\gamma_{50,x}^{(j)}$ are the same as Eq. (35), Eq. (37) ($k = 89, 88, j = 1, 2, \dots, 90$) and Eq. (36), respectively. And a 3D dynamic view is shown in Fig. 7 by Matlab.

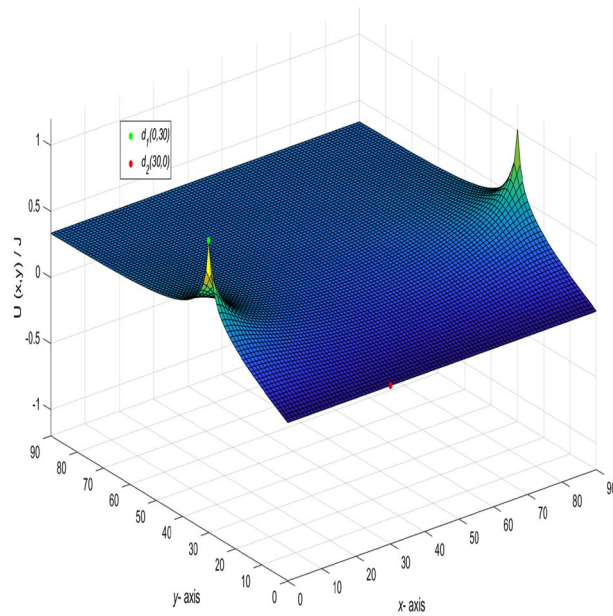


Figure 6. The process of forming a 3D dynamic view for $U_{90 \times 90}(x, y)/J$ in Eq. (42).

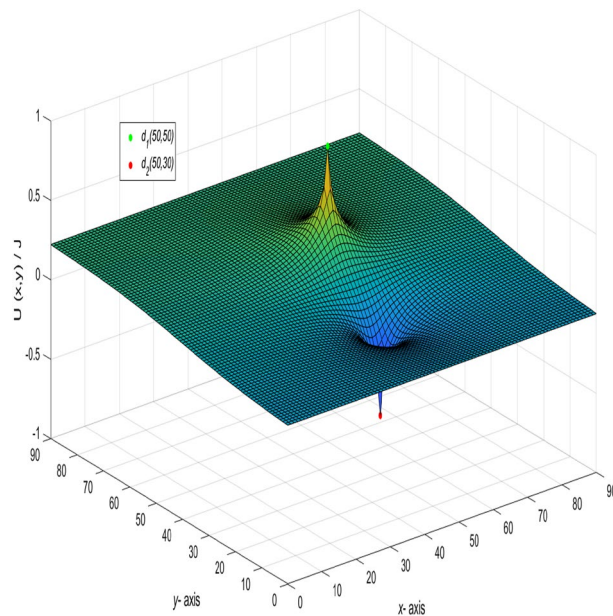


Figure 7. The process of forming a 3D dynamic view for $U_{90 \times 90}(x, y)/J$ in Eq. (44).

Special 5. When the current J enters from node $d_1(x_1, y_1)$ to node $d_2(x_2, y_1)$, in other words, $y_1 = y_2$. From Eq. (5), the potential of any node $d(x, y)$ can be written as

$$\frac{U_{m \times n}(x, y)}{J} = \frac{2r}{m} \sum_{j=2}^m \left(\frac{\gamma_{x_1, x}^{(j)} - \gamma_{x_2, x}^{(j)}}{t_j U_{n-1}^{(j)} - 2U_{n-2}^{(j)} - 2} \right) C_{y_1, j} C_{y, j}, \tag{46}$$

where $\gamma_{x_s, x_k}^{(j)}$, $U_k^{(j)}$ and $C_{k, j}$ are equal to Eq. (6), Eq. (9) and Eq. (7), respectively.

When $m = n = 90$, $J = 10$, $y_1 = y_2 = x_1 = 50$, $x_2 = 30$, and $r_0 = r = 1$, the following formula is obtained

$$\frac{U_{90 \times 90}(x, y)}{J} = \frac{1}{45} \sum_{j=2}^{90} \left(\frac{\gamma_{50, x}^{(j)} - \gamma_{30, x}^{(j)}}{t_j U_{89}^{(j)} - 2U_{88}^{(j)} - 2} \right) C_{50, j} C_{y, j}, \tag{47}$$

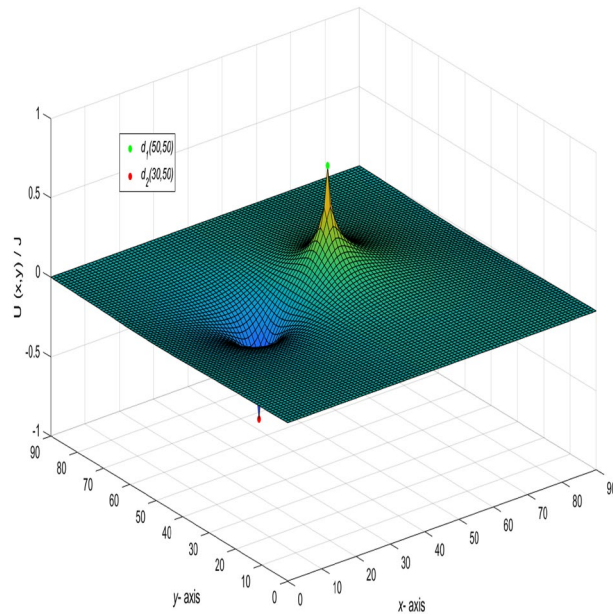


Figure 8. The process of forming a 3D dynamic view for $U_{90 \times 90}(x, y) / J$ in Eq. (47).

where $\gamma_{50,x}^{(j)}, \gamma_{30,x}^{(j)}, C_{50,j}, t_j$ and $U_k^{(j)}$ are the same as Eq. (36), Eq. (40), Eq. (45), Eq. (35) and Eq. (37), respectively, $k = 89 - |50 - x|, |50 - x| - 1, 89 - |30 - x|, |30 - x| - 1, 89, 88, j = 1, 2, \dots, 90$. And a 3D dynamic view is shown in Fig. 8 by Matlab.

Special 6. Presuming that $d_k(x_k, y_1) (k = 1, 2, \dots, k)$ entering the node at the same latitude is J/k and the current flowing out from $O(0, 0)$ is J , the potential equation is obtained.

$$\frac{U_{m \times n}(x, y)}{J} = r_0 \frac{yy_1}{mn} + \frac{2r}{km} \sum_{j=2}^m \frac{C_{y_1,j} C_{y_j}}{t_j U_{n-1}^{(j)} - 2U_{n-2}^{(j)} - 2} \sum_{s=1}^k \gamma_{x_s,x}^{(j)} \tag{48}$$

where $C_{k,j}, \gamma_{x_s,x_k}^{(j)}$ and $U_k^{(j)}$ are equal to Eq. (7), Eq. (6) and Eq. (9), respectively.

When $m = n = 90, J = 10, y_1 = y_2 = x_1 = 50, x_2 = 30, x_3 = 40, r_0 = r = 1$, and $k = 3$ the following formula is obtained

$$\frac{U_{90 \times 90}(x, y)}{J} = \frac{y}{162} + \frac{1}{45} \sum_{j=2}^{90} \frac{C_{50,j} C_{y_j}}{t_j U_{89}^{(j)} - 2U_{88}^{(j)} - 2} (\gamma_{50,x}^{(j)} + \gamma_{40,x}^{(j)} + \gamma_{30,x}^{(j)}), \tag{49}$$

$$\gamma_{40,x}^{(j)} = U_{89-|40-x|}^{(j)} + U_{|40-x|-1}^{(j)},$$

where $C_{50,j}, t_j, \gamma_{50,x}^{(j)}, \gamma_{30,x}^{(j)}$ and $U_k^{(j)}$ is defined in Eq. (45), Eq. (35), Eq. (36), Eq. (40) and Eq. (37) ($k = 89 - |50 - x|, |50 - x| - 1, 89 - |40 - x|, |40 - x| - 1, 89 - |30 - x|, |30 - x| - 1, 89, 88, j = 1, 2, \dots, 90$), respectively.

And a 3D dynamic view is shown in Fig. 9 by Matlab.

Fast numerical algorithm for computing potential

In order to realize fast calculation of potential for large-scale resistor networks. In this section, by summarizing the previous discussion and analysis, a fast numerical algorithm of computing potential by the Eqs. (8), (9), (10), (26), (27), (28), (29), (30), (31), (32) and the famous second type of discrete cosine transform (DCT-II) are given.

Algorithm 1: Fast matrix-vector multiplication $\mathbf{B}_m \mathbf{v} = \mathbf{y}$

- Step 1: Compute y_1 by the Eq. $y_1 = (2 + b)v_1 - bv_2$;
 - Step 2: Cycle computing y_i by the Eq. $y_i = (-b)v_{i-1} + (2 + 2b)v_i - bv_{i+1}, i = 2, \dots, m - 1$;
 - Step 3: Compute y_m by the Eq. $y_m = (-b)v_{m-1} + (2 + b)v_m$.
-

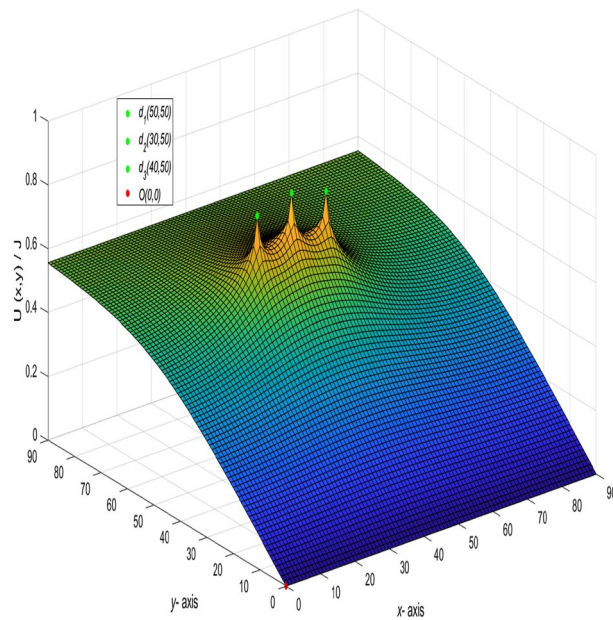


Figure 9. The process of forming a 3D dynamic view for $U_{90 \times 90}(x, y)/J$ in Eq. (49).

Algorithm 2: Fast algorithm for computing $U_{m \times n}(x, y)/J$

- Step 1: Compute t_j by Eq. (8), $j = 1, 2, \dots, m$;
 Step 2: Compute $\psi_j = \arccos(\frac{t_j}{2})$, $j = 1, 2, \dots, m$;
 Step 3: Compute $U_k^{(j)}$ by Eq. (9), $k = n - |x_t - x|$, $|x_t - x|$, $n - 1$, $n - 2$, $t = 1, 2$, $j = 1, 2, \dots, m$;
 Step 4: Compute $W_x^{(1)}$ by Eq. (31) and $W_x^{(j)}$ by Eq. (32), $x = 0, 1$; $j = 2, \dots, m$;
 Step 5: Compute \mathbf{I}_k by Eq. (29), (30) and DCT-II, $k = 0, 1$;
 Step 6: Compute $\mathbf{B}_m \mathbf{I}_k$ by Algorithm 1, $k = 1, 2, \dots$;
 Step 7: Cycle computing \mathbf{I}_k by Eq. (26), (27) and (28), $k = 2, 3, \dots$;
 Step 8: Compute $U_{m \times n}(x, y)/J$ by Eq. (10).
-

As is well known, the complexity of tridiagonal matrix-vector multiplication is $O(n)$, which is the same as Algorithm 1. Moreover, one DCT-II needs $2n \log_2 n + O(n)$ real arithmetic operations^{57,58}. So the complexity of Algorithm 2 is $4n \log_2 n + O(n)$ consist of two DCT-II and Algorithm 1.

According to the above two algorithms, two examples are used to vividly show the computational efficiency for the large scale globe resistor networks.

Example 1 In the network with $m = 1000$ and $n = 10$, the current flows in from $(x_1, y_1)(x_1 = 3, y_1 = 200)$ and out from $(x_2, y_2)(x_2 = 5, y_2 = 300)$, $r = 1$, $r_0 = 100$, and $J = 10$. The results calculated using Algorithm 2 are shown in Fig. 10.

Example 2 In the scale of $m \times n(300 \times 10)$, when the current $x_1 = 3$, $x_2 = 5$, $y_1 = 100$, $y_2 = 200$, and $r = 1$, $r_0 = 100$. The results calculated using Algorithm 2 are shown in Fig. 11.

Conclusions. This paper achieved a series of improved exact potential formulae in an $m \times n$ globe network by the $RT-I$ method. Chebyshev polynomial of the second kind is introduced to improve the potential formula of the globe network⁴⁴. Some applications of the new potential formula of the globe network are presented, such as some special and interesting potential formulae are given in Eqs. (33), (38), (41), (43), (46) and (48), respectively. The image numerical simulation using matlab has produced many interesting 3D dynamic views. Finally, we also put forward a fast numerical algorithm by the famous second type of discrete cosine transform, which can realize fast calculation of potential for large-scale resistor networks. Furthermore, by using our research ideas of resistor network, we can also explore neural networks¹¹⁻¹⁷. That will be our next step.

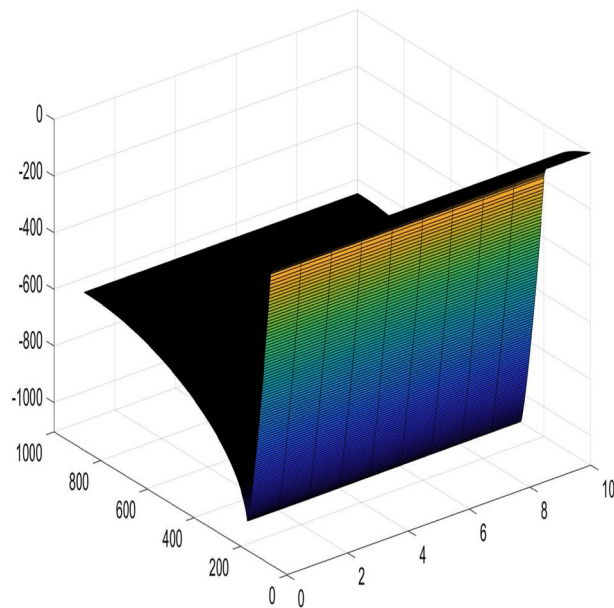


Figure 10. A 3D graph for the changes of $U_{1000 \times 10}(x, y)/J$ with x and y .

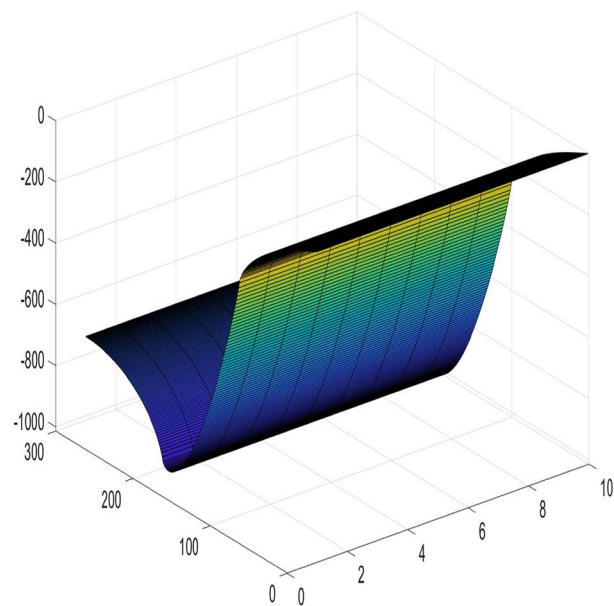


Figure 11. A 3D graph for the changes of $U_{300 \times 10}(x, y)/J$ with x and y .

Data availability

All data generated or analysed during this study are included in this article [and its supplementary information files].

Received: 30 September 2022; Accepted: 5 December 2022

Published online: 08 December 2022

References

1. Hadad, Y., Soric, J. C., Khanikaev, A. B. & Alù, A. Self-induced topological protection in nonlinear circuit arrays. *Nat. Electron.* **1**, 178–182 (2018).
2. Zhang, D. *et al.* Impact damage localization and mode identification of CFRPs panels using an electric resistance change method. *Compos. Struct.* **276**, 114587 (2021).
3. Kirchhoff, G. Ueber die Auflösung der Gleichungen, auf welche man bei der Untersuchung der linearen Vertheilung galvanischer Ströme geführt wird. *Ann. Phys.* **148**, 497–508 (1847).

4. Winstead, V. & Demarco, C. L. Network essentiality. *IEEE T. Circuits-I*. **60**(3), 703–709 (2012).
5. Ferri, G. & Antonini, G. Ladder-network-based model for interconnects and transmission lines time delay and cutoff frequency determination. *J. Circuit. Syst. Comp.* **16**, 489–505 (2007).
6. Owaitat, M. Q., Hijjawi, R. S. & Khalifeh, J. M. Network with two extra interstitial resistors. *Int. J. Theor. Phys.* **51**, 3152–3159 (2012).
7. Kirkpatrick, S. Percolation and conduction. *Rev. Mod. Phys.* **45**, 497–508 (1973).
8. Katsura, S. & Inawashiro, S. Lattice Green's functions for the rectangular and the square lattices at arbitrary points. *J. Math. Phys.* **12**, 1622 (1971).
9. Pennetta, C. *et al.* Biased resistor network model for electromigration failure and related phenomena in metallic lines. *Phys. Rev. B*. **70**, 174305 (2004).
10. Kook, W. Combinatorial Green's function of a graph and applications to networks. *Adv. Appl. Math.* **46**, 417–423 (2011).
11. Shi, Y. *et al.* Novel discrete-time recurrent neural networks handling discrete-form time-variant multi-augmented Sylvester matrix problems and manipulator application. *IEEE T. Neur. Net. Lear.* **33**(2), 587–599 (2022).
12. Shi, Y., Zhao, W.-H., Li, S., Li, B. & Sun, X.-B. Novel discrete-time recurrent neural network for robot manipulator: A direct discretization technical route. *IEEE T. Neur. Net. Lear.* <https://doi.org/10.1109/TNNLS.2021.3108050> (2021).
13. Liu, K.-P. *et al.* Five-step discrete-time noise-tolerant zeroing neural network model for time-varying matrix inversion with application to manipulator motion generation. *Eng. Appl. Artif. Intel.* **103**, 104306 (2021).
14. Sun, Z.-B. *et al.* Noise-suppressing zeroing neural network for online solving time-varying matrix square roots problems: A control-theoretic approach. *Expert. Syst. Appl.* **192**, 116272 (2022).
15. Jin, L., Qi, Y.-M., Luo, X., Li, S. & Shang, M.-S. Distributed competition of multi-robot coordination under variable and switching topologies. *IEEE T. Autom. Sci. Eng.* **19**(4), 3575–3586 (2022).
16. Jin, L., Zhang, Y.-N., Li, S. & Zhang, Y.-Y. Modified ZNN for time-varying quadratic programming with inherent tolerance to noises and its application to kinematic redundancy resolution of robot manipulators. *IEEE T. Ind. Electron.* **63**(11), 6978–6988 (2016).
17. Jin, L., Zheng, X. & Luo, X. Neural dynamics for distributed collaborative control of manipulators with time delays. *IEEE-CAA J. Autom.* **9**(5), 854–863 (2022).
18. Klein, D. J. & Randić, M. Resistance distance. *J. Math. Chem.* **12**, 81–95 (1993).
19. Cserti, J. Application of the lattice Green's function for calculating the resistance of an infinite network of resistors. *Am. J. Phys.* **68**, 896–906 (2000).
20. Giordano, S. Disordered lattice networks: General theory and simulations. *Int. J. Circ. Theor. Appl.* **33**, 519–540 (2005).
21. Wu, F. Y. Theory of resistor networks: The two-point resistance. *J. Phys. A Math. Gen.* **37**, 6653 (2004).
22. Tzeng, W. J. & Wu, F. Y. Theory of impedance networks: The two-point impedance and LC resonances. *J. Phys. A Math. Gen.* **39**, 8579 (2006).
23. Essam, J. W. & Wu, F. Y. The exact evaluation of the corner-to-corner resistance of an $M \times N$ resistor network: Asymptotic expansion. *J. Phys. A Math. Theor.* **42**, 025205 (2008).
24. Izmailian, N. S. & Huang, M.-C. Asymptotic expansion for the resistance between two maximum separated nodes on an M by N resistor network. *Phys. Rev. E*. **82**, 011125 (2010).
25. Lai, M.-C. & Wang, W.-C. Fast direct solvers for Poisson equation on 2D polar and spherical geometries. *Numer. Meth. Part. D. E.* **18**, 56–68 (2002).
26. Borges, L. & Daripa, P. A fast parallel algorithm for the Poisson equation on a disk. *J. Comput. Phys.* **169**, 151–192 (2001).
27. Izmailian, N. S., Kenna, R. & Wu, F. Y. The two-point resistance of a resistor network: A new formulation and application to the cobweb network. *J. Phys. A Math. Theor.* **47**, 035003 (2014).
28. Izmailian, N. S. & Kenna, R. A generalised formulation of the Laplacian approach to resistor networks. *J. Stat. Mech: Theor. E*. **9**, 1742–5468 (2014).
29. Izmailian, N. S. & Kenna, R. The two-point resistance of fan networks. *Chin. J. Phys.* **53**(2), 040703 (2015).
30. Chair, N. Trigonometrical sums connected with the chiral Potts model, verlinde dimension formula, two-dimensional resistor network, and number theory. *Ann. Phys.* **341**, 56–76 (2014).
31. Chair, N. The effective resistance of the N -cycle graph with four nearest neighbors. *J. Stat. Phys.* **154**, 1177–1190 (2014).
32. Tan, Z.-Z., Zhou, L. & Yang, J.-H. The equivalent resistance of a $2 \times n$ cobweb network and its conjecture of an $m \times n$ cobweb network. *J. Phys. A Math. Theor.* **46**(19), 195202 (2013).
33. Tan, Z.-Z. Recursion-transform approach to compute the resistance of a resistor network with an arbitrary boundary. *Chin. Phys. B*. **24**(2), 020503 (2015).
34. Tan, Z.-Z. Recursion-transform method for computing resistance of the complex resistor network with three arbitrary boundaries. *Phys. Rev. E*. **91**(5), 052122 (2015).
35. Tan, Z.-Z. Recursion-transform method to a non-regular $m \times n$ cobweb with an arbitrary longitude. *Sci. Rep.* **5**, 11266 (2015).
36. Tan, Z.-Z., Essam, J. W. & Wu, F. Y. Two-point resistance of a resistor network embedded on a globe. *Phys. Rev. E*. **90**(1), 012130 (2014).
37. Essam, J. W., Tan, Z.-Z. & Wu, F. Y. Resistance between two nodes in general position on an $m \times n$ fan network. *Phys. Rev. E*. **90**(3), 032130 (2014).
38. Tan, Z.-Z. & Fang, J.-H. Two-point resistance of a cobweb network with a $2r$ boundary. *Commun. Theor. Phys.* **63**(1), 36–44 (2015).
39. Tan, Z.-Z. Theory on resistance of $m \times n$ cobweb network and its application. *Int. J. Circ. Theor. Appl.* **43**(11), 1687–1702 (2015).
40. Tan, Z.-Z. Two-point resistance of a non-regular cylindrical network with a zero resistor axis and two arbitrary boundaries. *Commun. Theor. Phys.* **67**(3), 280–288 (2017).
41. Tan, Z.-Z. Two-point resistance of an $m \times n$ resistor network with an arbitrary boundary and its application in RLC network. *Chin. Phys. B*. **25**(5), 050504 (2016).
42. Tan, Z.-Z. Recursion-transform method and potential formulae of the $m \times n$ cobweb and fan networks. *Chin. Phys. B*. **26**(9), 090503 (2017).
43. Tan, Z., Tan, Z.-Z. & Chen, J. Potential formula of the nonregular $m \times n$ fan network and its application. *Sci. Rep.* **8**, 5798 (2018).
44. Tan, Z. & Tan, Z.-Z. Potential formula of an $m \times n$ globe network and its application. *Sci. Rep.* **8**(1), 9937 (2018).
45. Fu, Y.-R., Jiang, X.-Y., Jiang, Z.-L. & Jhang, S. Properties of a class of perturbed Toeplitz periodic tridiagonal matrices. *Comp. Appl. Math.* **39**, 1–19 (2020).
46. Fu, Y.-R., Jiang, X.-Y., Jiang, Z.-L. & Jhang, S. Inverses and eigenpairs of tridiagonal Toeplitz matrix with opposite-bordered rows. *J. Appl. Anal. Comput.* **10**(4), 1599–1613 (2020).
47. Fu, Y.-R., Jiang, X.-Y., Jiang, Z.-L. & Jhang, S. Analytic determinants and inverses of Toeplitz and Hankel tridiagonal matrices with perturbed columns. *Spec. Matrices*. **8**, 131–143 (2020).
48. Wei, Y.-L., Zheng, Y.-P., Jiang, Z.-L. & Shon, S. The inverses and eigenpairs of tridiagonal Toeplitz matrices with perturbed rows. *J. Appl. Math. Comput.* **68**, 623–636 (2022).
49. Wei, Y.-L., Jiang, X.-Y., Jiang, Z.-L. & Shon, S. On inverses and eigenpairs of periodic tridiagonal Toeplitz matrices with perturbed corners. *J. Appl. Anal. Comput.* **10**(1), 178–191 (2020).
50. Wei, Y.-L., Zheng, Y.-P., Jiang, Z.-L. & Shon, S. A study of determinants and inverses for periodic tridiagonal Toeplitz matrices with perturbed corners involving Mersenne numbers. *Mathematics* **7**(10), 893 (2019).

51. Wei, Y.-L., Jiang, X.-Y., Jiang, Z.-L. & Shon, S. Determinants and inverses of perturbed periodic tridiagonal Toeplitz matrices. *Adv. Differ. Equ.* **2019**(1), 410 (2019).
52. Udreă, G. A note on the sequence $(W_n)_{n \geq 0}$ of A.F. Horadam. *Port. Math.* **53**, 143–156 (1996).
53. Mason, J. C. & Handscomb, D. C. *Chebyshev Polynomials* (Chapman and Hall/CRC, Boca Raton, 2002).
54. Garcia, S. R. & Yih, S. Supercharacters and the discrete Fourier, cosine, and sine transforms. *Commun. Algebra.* **46**(9), 3745–3765 (2018).
55. Sanchez, V., Garcia, P., Peinado, A. M., Segura, J. C. & Rubio, A. J. Diagonalizing properties of the discrete cosine transforms. *IEEE T. Signal. Process.* **43**(11), 2631–2641 (1995).
56. Strang, G. The discrete cosine transform. *SIAM. Rev.* **41**(1), 135–147 (1999).
57. Liu, Z., Chen, S., Xu, W. & Zhang, Y. The eigen-structures of real (skew) circulant matrices with some applications. *Comput. Appl. Math.* **38**, 178 (2019).
58. Yip, P. C. & Rao, K. R. DIF algorithms for DCT and DST. *IEEE Int. Conf. Acoust. Speech. Signal Process.* <https://doi.org/10.1109/ICASSP.1985.1168246> (1985).

Acknowledgements

The research was Supported by the National Natural Science Foundation of China (Grant No. 12001257), the Natural Science Foundation of Shandong Province (Grant No. ZR2020QA035).

Author contributions

Y.-P.Z. and X.-Y.J. conceived the project, performed and analyzed formulae calculations. Y.-F.Z. validated the correctness of the calculations. Z.-L.J. present the fast algorithm for solving the matrix equation. All authors contributed equally to the manuscript.

Competing interests

The authors declare no competing interests.

Additional information

Supplementary Information The online version contains supplementary material available at <https://doi.org/10.1038/s41598-022-25724-y>.

Correspondence and requests for materials should be addressed to Y.Z. or Z.J.

Reprints and permissions information is available at www.nature.com/reprints.

Publisher's note Springer Nature remains neutral with regard to jurisdictional claims in published maps and institutional affiliations.



Open Access This article is licensed under a Creative Commons Attribution 4.0 International License, which permits use, sharing, adaptation, distribution and reproduction in any medium or format, as long as you give appropriate credit to the original author(s) and the source, provide a link to the Creative Commons licence, and indicate if changes were made. The images or other third party material in this article are included in the article's Creative Commons licence, unless indicated otherwise in a credit line to the material. If material is not included in the article's Creative Commons licence and your intended use is not permitted by statutory regulation or exceeds the permitted use, you will need to obtain permission directly from the copyright holder. To view a copy of this licence, visit <http://creativecommons.org/licenses/by/4.0/>.

© The Author(s) 2022